Green Carbon 4 (2026) 27–33

Contents lists available at ScienceDirect

Green Carbon

journal homepage: www.keaipublishing.com/en/journals/green-carbon/

Research Article

Facile functionalization of ZIF–8 *via* mechanochemical post-synthetic linker exchange for improved CO_2 capture performance

Aljaž Škrjanc[a,b], Nataša Zabukovec Logar[a,b,*]

[a] National Institute of Chemistry, Hajdrihova 19, Ljubljana SI-1001, Slovenia
[b] University of Nova Gorica, Vipavska 13, Nova Gorica SI-5000, Slovenia

ARTICLE INFO

Keywords:
CO_2 capture
Mechanochemistry
Post-synthetic modification
Zeolitic imidazolate frameworks

ABSTRACT

Effective CO_2 capture is one of the crucial prerequisites for successful carbon management. The development of metal-organic frameworks (MOFs) and their subgroup, zeolitic imidazolate frameworks (ZIFs), have emerged as prominent materials in CO_2 capture research. Among these, the most widely studied and utilized ZIF is the zinc 2-methylimidazolate with sodalite topology known as ZIF–8. Despite its exceptionally high porosity and stability under hydrothermal and chemical conditions, ZIF–8 has shown limited utility as a CO_2 adsorbent due to its low uptake capacity. This limitation is primarily attributed to the absence of polar functional groups in the framework, reducing interactions between the framework and CO_2. With the growing interest in mechanochemistry for the synthesis of reticular materials, we explored the incorporation of linkers with polar groups using mechanical forces. Initially, we focused on a system based on ZIF–8 and imidazole-2-carboxaldehyde as polar exchange linker. The optimal conditions, which achieved linker exchange of up to 63% within 15 min, were subsequently tested with four additional imidazole linkers with 4-carbaldehyde, hydroxide, and chloride functional groups. The synthesized materials were evaluated as CO_2 sorbents, and further experimental evidence was found for the significance of the position of the polar functional group in the imidazolate ring for CO_2 sorption in sodalite ZIFs.

1. Introduction

Zeolitic imidazolate frameworks (ZIFs) are a subgroup of metal–organic frameworks (MOFs), which consist of tetrahedrally coordinated single metal nodes linked together with imidazole- and benzimidazole-based linkers [1]. The strong coordination bonds between the imidazolate linkers and metal ions, together with the preferential formation of rigid cages, make ZIFs highly robust and permanently porous materials. Their similarity to aluminosilicate zeolites is attributed to the similar bond angles and topologies of their frameworks [2]. The most widely studied and utilized ZIF is the zinc 2-methylimidazolate framework with sodalite (SOD) topology, known as ZIF–8 [3,4].

Despite its high porosity, excellent thermal [5], hydrothermal [6], and chemical [7] stability, as well as commercial availability, ZIF–8 has not been widely used as a CO_2 adsorbent owing to its low uptake compared to some other ZIFs, MOFs, and porous carbons [8]. The low CO_2 uptake of ZIF–8 can be attributed to the lack of dipoles (polar functional groups) in the framework, which consists of 2-methylimidazolate linkers bonded *via* Zn-ion nodes. This leads to reduced interaction between the framework and CO_2 [9–11] compared to other ZIFs with the same framework topology but different or additional functional groups on the ligands [10].

In recent years, various mixed linker (ML) systems with ZIF–8 have been developed with the aim of enhancing framework CO_2 interactions and thereby increasing the CO_2 uptake [12–15]. When direct synthesis of ML–ZIF–8 with desired topology and functionality is not achievable due to general thermodynamic/kinetic obstacles towards framework formation, post-synthetic functionalization can be a viable alternative. For this purpose, the most widely utilized method for ZIF–8 is linker exchange *via* solvent-assisted ligand exchange (SALE) [16–18].

The SALE of Cd-based ZIFs was first reported in 2012 [19]. The authors found that, by soaking the formed framework in a solution of another linker at slightly elevated temperatures, an exchange of linkers

Peer review under the responsibility of Editorial Office of Qingdao Institute of Bioenergy and Bioprocess Technology, Chinese Academy of Sciences.
* Corresponding author.
E-mail address: natasa.zabukovec@ki.si (N.Z. Logar).

https://doi.org/10.1016/j.greenca.2025.06.002
Received 26 February 2025; Received in revised form 19 May 2025; Accepted 5 June 2025
Available online 25 July 2025

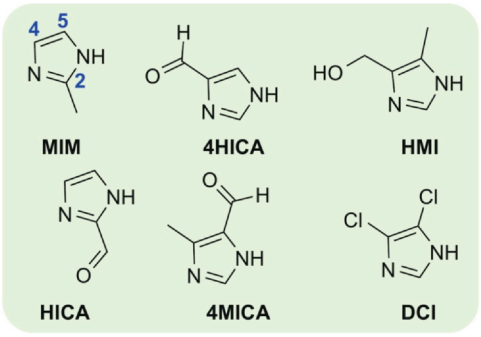

Fig. 1. Imidazoles used in the present study and their abbreviations. MIM, 2-methyl imidazole; 4HICA, 4-Imidazolecarboxaldehyde; HMI, 4-Hydroxymethyl-5-methylimidazole; HICA, 2-imidazolecarboxaldehyde; 4MICA, 4-Methyl-5-imidazolecarboxaldehyde; DCl, 4,5-Dichloroimidazole. MIM has the imidazole ring positions labelled in blue.

occurred. While no major change was observed in the powder X-ray diffracton (PXRD) patterns, a slight decrease in the unit cell length and surface area was observed. In the case of CdIF-4, most linkers were exchanged after 48 h. Afterwards, reversibility tests were performed, and it was found that in some cases, SALE was reversible, that is, soaking in the initial linker could restore the original ZIF [19].

SALE was quickly transferred to use with the Zn-based ZIF–8 [16,18,20,21]. The chosen linkers differed mainly in the functional groups at the 2-position of the imidazole ring (Fig. 1), with the base linkers being either pure imidazole or benzimidazole. The authors varied the solvent composition, time, and temperature to achieve the desired results of maintaining the initial SOD topology. The reaction times varied from a few hours to a week. While the original SALE procedure for CdIF-4 exhibited reversibility, no such reversibility has been observed for the SALE of ZIF–8. Furthermore, due to the commercial availability of ZIF–8, SALE was recognized as an efficient way to implement functionality into a ZIF with SOD topology. However, the main disadvantage of SALE is the common use of DMF as the solvent and prolonged synthesis times.

With the rise of mechanochemistry, ligand exchange using mechanical forces has been tested and has shown promise for a system based on ZIF–8. Jiang *et al.* [17] managed to introduce six imidazole linkers with varying functional groups replacing the 2-methyl imidazole linkers of the parent ZIF–8 by neat grinding in a mortar and pestle. The small mechanical forces achieved with hand grinding required prolonged grinding times of up to 8 h, which is still significantly shorter than the multiple days required for most SALE. The resulting linker exchanges in the Jiang's report were either comparable to or higher than those reported for the three-day SALE procedure.

The mechanochemically assisted ligand-exchange approach (MALE) was subsequently extended to carboxylate MOFs such as UiO-66 [17,22] and MOF-808. Notably, a key advancement was the demonstration that MALE can be a reversible process in Zn ZIF systems [17], enabling more precise control of the linker ratios, further proving that MALE can be a path towards the preparation of novel ZIF materials.

Herein, we report the preparation of a series of ML ZIF–8-based compounds, where ball-mill MALE conditions were first investigated with ZIF–8 and imidazole-2-caboxaldehyde as the exchanging linker (HICA) (Fig. 1); the MALE reaction time was reduced by more than 30 times, from hours to minutes. The optimal MALE conditions were then applied to four functionalized imidazoles, functionalized at the 4 or 5 position (Fig. 1), which are known to exhibit higher affinity for CO_2 compared to position 2-substituted at lower pressures [23], but have difficulties in forming highly porous SOD frameworks under solvothermal conditions or do not have known SOD phases at all. The obtained materials were then evaluated as CO_2 capture materials.

2. Materials and methods

2.1. Materials

2-Methylimidazole (MIM, 99%) and Zinc nitrate hexahydrate (Zn $(NO_3)_2$•$6H_2O$) were purchased from Sigma-Aldrich, 4-Imidazolecarboxaldehyde (4HICA, 95%), 4-Methyl-5-imidazolecarboxaldehyde (4MICA, 97%), 4-Hydroxymethyl-5-methylimidazole (HMI, 95%), and 2-imidazolecarboxaldehyde (HICA, 95%) were purchased from Fluorochem. Methanol (MeOH, 99.9%) was purchased from Honeywell. 4,5-Dichloroimidazole (DCl, 98%) was obtained from ABCR. Ethanol (EtOH, 96%) was purchased from Stella TECH. All the chemicals were used as such without further purification.

2.2. Synthesis

2.2.1. ZIF–8 nanoparticles

A solution of 1.51 g (4.6 mmol) of zinc nitrate hexahydrate in 50 mL of MeOH was added to a solution of 3.33 g (4 mmol) of MIM in 50 mL of MeOH. The combined solutions were left to stir covered for 24 h and then centrifuged at 6000 rpm. The precipitate was then resuspended in fresh EtOH and centrifuged. The samples were then dried in a fan oven at 60 ˚C overnight.

2.2.2. MALE procedure

ZIF–8 was added to a stainless-steel grinding jar, followed by the addition of the second linker. Stainless-steel grinding balls were added, and the milling was done according to the conditions described in Table 1 with a milling time of 15 min using a Retsch MM400 mill. After milling, the samples were washed twice with EtOH by suspending them in 10 mL of EtOH, followed by centrifugation. In the case of MALE procedure by liquid assisted grinding (LAG-20 samples), 100 µl of EtOH was added to the ZIF–8 and linker before milling with 10 mm grinding balls.

2.3. Characterization

PXRD data were recorded on a PANanalytical X'Pert PRO high-resolution diffractometer using Cu $K_{\alpha 1}$ radiation (1.5406 Å) in the 2θ range, 5˚–50˚ (100 s per step 0.033˚ 2θ) with a fully opened X'Celerator detector. The crystallite size was determined using the built in Scherrer calculator in X' Pert High Score software.

Nitrogen physisorption isotherms were recorded at −196 ˚C using an Autosorb iQ3 instrument. Before the adsorption analysis, the samples were degassed under vacuum at 150 ˚C. The Brunauer–Emmett–Teller (BET) specific surface area was calculated from the adsorption data in the relative pressure range 0.005–0.02. The total pore volume (V_{total}) was calculated from the amount of N_2 adsorbed at $p/p_0 = 0.97$ and micropore volume as calculated from t-plot (p/p_0 = 0.15–0.3) using the built-in software using the deBoer model.

The acid-digestion liquid ^{1}H NMR spectra were recorded using an AVANCE NEO Bruker 600 MHz spectrometer at room temperature. Approximately 1.5 mg of each sample was digested in a mixture of DCl (35%) and D_2O (0.1 mL) and diluted with DMSO-d_6 (0.5 mL). Data analysis was performed using TopSpin 4.3.0 (Bruker). Scanning electron microscope (SEM) images were taken using a Zeiss Supra 35 VP microscope.

The CO_2 isotherms were collected on a Surface Measurements Systems DVS Vacuum system. The samples were first degassed at 100 ˚C in a vacuum with the turbo pump on for 60 min and then left to cool under vacuum for 3 h. The isotherms were collected at 25 ˚C in the pressure range of 0–1 bar.

3. Results and discussion

The parent nanosized ZIF–8 was prepared and characterized by PXRD and SEM (Fig. S1). These results confirmed the absence of ZIF–L [24] crystals or potential alternative polymorphs of zinc 2-methylimidazolate

Table 1
MALE conditions. The obtained products are named after the linker (Fig. 1) and the milling frequency used. The rate of ligand exchange was determined based on acid digestion ^{1}H liquid NMR peak integrals. Due to the overlap of the rapid exchange proton peak in the NMR spectra with the HICA peak at 7.5 ppm, the peak at 6 ppm was used. The integrals for both HICA peaks were in all cases 2:1 as would be expected.

	ZIF–8 (mg)	MALE linker (mg)	Linker/ZIF ratio	Jar (mL)	Balls (mm)	Frequency (Hz)	Halved integral of ring protons of MIM [a,b]
HICA – 10A	50	50	1	10	10	10	15.50
HICA – 10B	50	100	2	10	10	10	13.75
HICA-10C	100	100	1	25	15	10	11.35
HICA – 10D	100	200	2	25	15	10	9.90
HICA – 20A	50	50	1	10	10	20	0.96
HICA – 20B	50	100	2	10	10	20	1.50
HICA–20C	100	100	1	25	15	20	0.60
HICA – 20D	100	200	2	25	15	20	0.85
HICA – 30A	50	50	1	10	10	30	0.80
HICA – 30B	50	100	2	10	10	30	0.85
HICA–30C	100	100	1	25	15	30	0.60
HICA – 30D	100	200	2	25	15	30	0.55
4HICA – 20[c]	100	100	1	25	15	20	0.835
4MICA – 20[d]	100	100	1	25	15	20	1.00
HMI – 20[e]	100	100	1	25	15	20	2.50
DCl – 20	100	100	1	25	15	20	0.27

[a] Integral of second linker was calibrated to 1.
[b] The integral was normalized to 1 proton.
[c] The peak at 9.7 ppm was chosen.
[d] The peak at 9.8 ppm was chosen.
[e] HMI-20(10) used 10 mm grinding balls, NMR peaks of methyl groups were chosen for LAG samples.

[25]. The methanol used in the synthesis was recovered using a rotary evaporator to reduce liquid waste. ^{1}H NMR spectrum of the recovered solvent (Fig. S2) showed that it was sufficiently pure for further use in the subsequent ML ZIF–8 synthesis.

3.1. MALE with HICA: condition screening

After the successful synthesis of ZIF–8 nanoparticles, the ZIF and selected MALE linkers were weighed into milling jars, and MALE was done using ball milling for 15 min, based on our previous experience [23,26]. We tested four potential jar "loadings" working in pairs, with one pair having a weight ratio of ZIF/Linker of 1/1 and the other of 1/2. Various frequencies were tested at the selected time, where 15 min provided sufficient reaction time without severe mechanochemical framework degradation. The milling conditions are listed in Table 1. For all three tested frequencies (10, 20, and 30 Hz), the highest exchange was observed when the weight/volume ratio (reagent mass to jar volume) was 8 or 12. While ligand exchange was very small at 10 Hz, a drastic increase in exchange was observed when 20 Hz was used (a jump from $<$ 10% to $>$ 40% exchange). A slightly smaller exchange was observed when shifting the frequency from 20 to 30 Hz. As anticipated, the trend was higher frequency, higher linker exchange, higher loss of crystallinity, and higher mesoporosity (Fig. 2 and Table 2).

The samples porosity was investigated with N_2 physisorption (Fig. 3 and Table 2). While a significant drop in surface area was observed compared to the as-synthesized parent ZIF–8, all determined S_{BET} values were within the range of the reported as-synthesized solvothermally pure HICA ZIF (ZIF–90), which tends to range from 600 to 1200 m^2/g.

The samples were then evaluated as single-component CO_2 sorbents (Fig. 4 and Table 2). In all cases, a linear adsorption isotherm was observed, with notable differences in the slopes of the curves depending on the degree of functionalization through linker exchange for a particular sample. A linear adsorption curve is characteristic for ZIF–8 (pure 2-methyl imidazolate) as well as the majority of other 2-substituted SOD ZIFs. Among the 12 samples prepared, the highest uptakes were observed for the HICA–30C (1.33 mmol/g) and HICA–30A (1.23 mmol/g) samples prepared at 30 Hz and the HICA–20C (1.25 mmol/g) sample prepared at 20 Hz.

Although, literature reports that mixed linker ZIF–8/90 systems with ZIF–90 being pure HICA (2-imidazolecarboxaldehyde) ZIF should have a higher CO_2 uptake than the individual components [12], this trend was not observed for our MALE samples. This could be attributed to different factors, including partial framework degradation from milling and its subsequent lower S_{BET}, possible pore

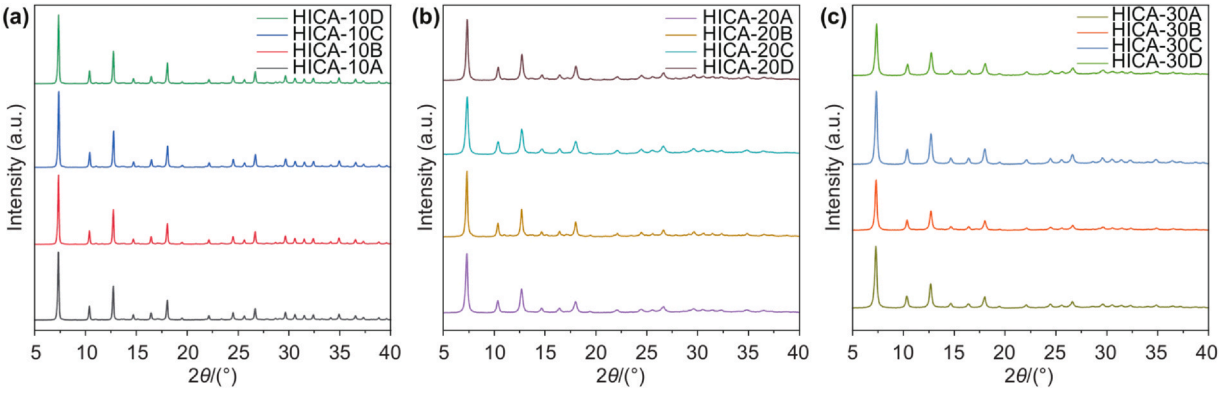

Fig. 2. PXRD of HICA MALE ZIF samples milled at **(a)** 10 Hz, **(b)** 20 Hz, and (c) 30 Hz, showing the trend of decreasing crystallinity with longer milling times.

Table 2
Weight/volume ratios of reagent mass to jar volume (w/V), linker exchange amount (determined by ^{1}H liquid NMR), and full width at half maximum (FWHM) of PXRD for MALE HICA samples. Numbers in names denote the milling frequency used.

	w/V (g/L)	Linker exchange (%)	FWMH (°)	Crystallite size (Å)	S_{BET} (m^2/g)	V_{micro} (mL/g)	V_{total} (mL/g)	CO_2 uptake at 25 °C (mmol/g)
HICA – 10A	10	6	0.13	1100	921	0.34	0.49	0.51
HICA – 10B	15	7	0.13	1170	975	0.37	0.56	0.67
HICA – 10C	8	8	0.13	1080	988	0.37	0.51	0.72
HICA – 10D	12	9	0.13	1120	1017	0.38	0.55	0.68
HICA – 20A	10	51	0.25	470	877	0.26	0.69	1.12
HICA – 20B	15	40	0.21	640	657	0.21	0.61	0.98
HICA – 20C	8	63	0.29	380	753	0.19	0.63	1.25
HICA – 20D	12	54	0.24	520	635	0.19	0.61	1.01
HICA – 30A	10	56	0.27	430	906	0.27	0.94	1.23
HICA – 30B	15	54	0.24	530	680	0.21	0.83	0.95
HICA – 30C	8	63	0.25	443	827	0.19	0.68	1.33
HICA – 30D	12	65	0.27	421	639	0.20	0.66	0.89

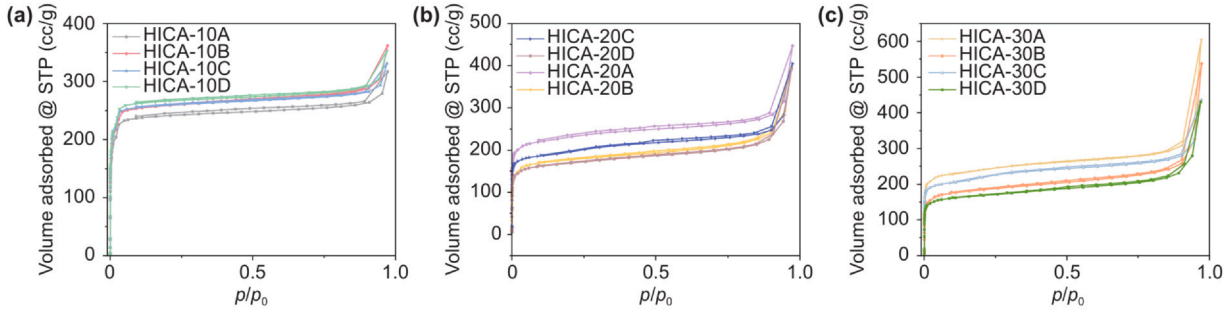

Fig. 3. N_2 isotherms of prepared HICA MALE samples milled at **(a)** 10 Hz, **(b)** 20 Hz, and **(c)** 30 Hz.

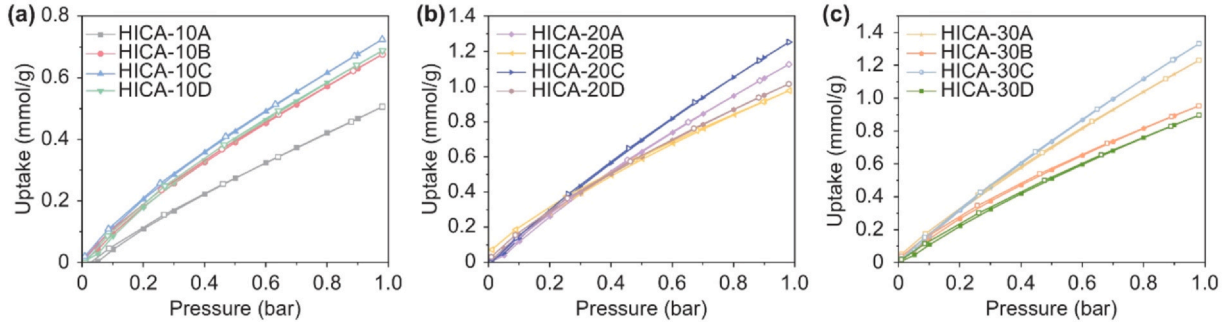

Fig. 4. CO_2 adsorption isotherms at 25 °C for HICA MALE samples milled at **(a)** 10 Hz, **(b)** 20 Hz, and **(c)** 30 Hz.

filling with excess linkers, and the lack of amines from DMF solvent decomposition, which usually cause higher reported uptakes than those of DMF-free (greener) alternatives such as methanol-prepared ZIF–8 [12,27,28].

Among the milling conditions tested at 20 Hz, those for HICA–20C were chosen for further MALE experiments. Although HICA–30C showed a slightly higher uptake, the higher frequency could potentially cause issues with the other selected functionalized linkers, leading us to err on the side of caution.

3.2. MALE with other imidazoles

Four imidazoles (Fig. 1) with polar functional groups were tested for potential incorporation into the ZIF–8 framework by MALE.

Of the tested linkers, only one case of MALE led to the retention of the SOD topology (Fig. 5). Both 5-methyl linkers (4MICA and HMI) decomposed into ZnO after the milling procedure, with the carboxaldehyde (4MICA) still retaining some visible diffraction peaks belonging to the SOD framework in the PXRD pattern.

In contrast, the dichloro linker (DCl) induced near-complete recrystallization into the highly porous RHO phase of ZIF–71 without the characteristic lsc pattern associated with ZIF–72. Some characteristic SOD peaks can still be observed as a shoulder of the peak at 7.3° 2θ (Fig. 5(b)). The results revealed that the milling conditions tested here were still slightly too harsh for more liable frameworks.

All samples were analyzed using acid digestion ^{1}H NMR (Table 3). The determined linker exchanges (Table 3) were somewhat in line with the observed PXRD results; DCl–20 had the highest determined exchange (78%, with recrystallization into the RHO topology), while HMI-20 had the lowest (29%, transformation into amorphous phase and ZnO). Both 4HICA–20 and 4MICA–20 had a determined linker ratio of approximately 1:1; that is, 50% exchange was observed. The samples, with the exception of HMI–20, were then tested for permanent porosity, and their CO_2 isotherms were collected (Fig. 5(c, d)). Notably, there is a change in the shape of the isotherms in the case of the 4-aldehyde linkers. Both 4MICA–20 and 4HICA–20 exhibited more prominent Langmuir-type isotherms than the linear isotherms observed for MALE –DCl and the 2-carboxaldehyde MALE samples (Table 2). The

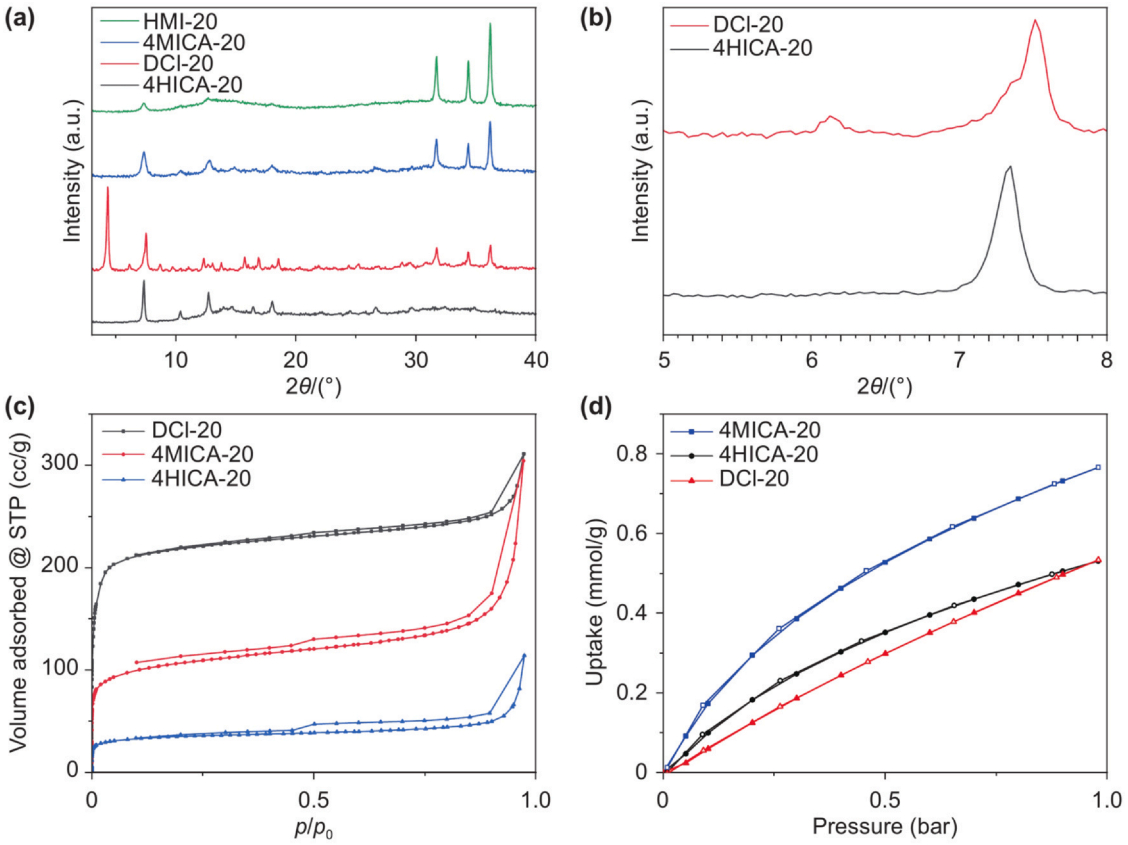

Fig. 5. **(a)** PXRD of MALE samples with HMI, 4MICA, DCI, and 4HICA. **(b)** PXRD of DCl–20 and 4HICA–20, magnified in the 5–8 2θ region. **(c)** N_2 physisorption and **(d)** CO_2 isotherms of MALE–20 samples with HIM, 4HICA, and 4MICA linkers incorporation.

Table 3
^{1}H NMR determined linker exchange and sorption results for the MALE samples with other linkers.

Sample	Linker exchange (%)	S_{BET} (m^2/g)	V_{micro} (mL/g)	V_{total} (mL/g)	CO_2 uptake (mmol/g)
4HICA – 20	54	126	0.04	0.18	0.53
4MICA – 20	50	385	0.11	0.47	0.77
HMI – 20	28	/	/	/	/
DCl – 20	79	858	0.28	0.48	0.53

comparably high CO_2 uptake of 4MICA–20 is also in line with the high uptake of its SOD pure linker zinc framework ZIF–94 [29]. While an increase in CO_2 affinity can be observed the loss of porosity due to partial structural collapse, subsequently leads to reduced uptake, which would otherwise be expected for the determined high linker ratio.

3.3. Liquid-assisted grinding-MALE

Given the high loss in crystallinity observed for MALE with 4HICA–20, 4MICA–20, and HMI–20 (Fig. 5(a)), we first attempted to determine whether the decomposition into ZnO could be stopped.

HMI–20 was chosen as the test system because it exhibited the lowest MALE stability under the tested conditions. The first step involved the use of smaller grinding balls (15–10 mm). The change to smaller grinding balls led to high amorphization of the SOD framework (Fig. 6(a)); however, this was significantly less than that previously observed for the HMI–20 sample.

The second approach tested was liquid-assisted grinding (LAG). The experiment led to a significantly better crystallinity of the LAG–HMI–20 sample compared to that of the HMI–20 sample (Fig. 6(a)). LAG was further tested using 4HICA and 4MICA (Fig. 6(a)). In the case of 4MICA, comparable crystallinity was observed as with MALE, while in the case of 4HICA, the crystallinity loss was more apparent and accompanied by the appearance of an additional PXRD peak at 14° 2θ.

The properties of the LAG–20 samples are listed in Table 4. The determined linker ratio was lower in all LAG–MALE samples than in MALE samples. Nitrogen physisorption (Fig. 6(b), Table 4) showed the expected decrease in S_{BET} with increasing linker exchange, owing to the larger functional groups of the selected exchanging linkers. In spite of lower S_{BET}, the CO_2 isotherms (Fig. 6(c)) revealed that both LAG–4HICA–20 and LAG–4MICA–20 samples show an increase in uptake if compared to 4HICA–20 and 4MICA–20 (0.75 *vs.* 0.53 mmol/g and 1.08 *vs.* 0.76 mmol/g, respectively), with both still exhibiting the expected Langmuir type isotherm shape of 4-aldehyde substituted imidazole ZIFs. We can conclude that with LAG–MALE we get reduced linker exchange compared to MALE. However, the lower amorphization and consequently higher porosity of the framework, leads to a higher CO_2 uptake.

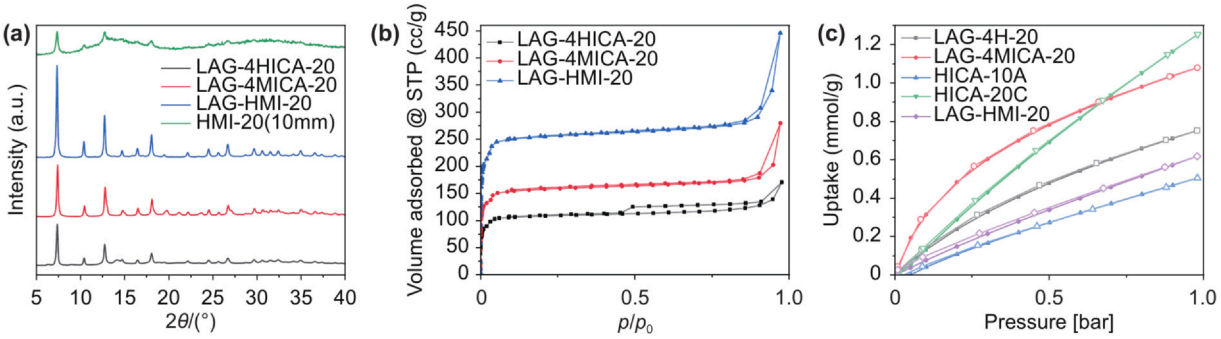

Fig. 6. (a) PXRD of HMI–20 (10 mm balls) and the LAG–20 samples. **(b)** N_2 physisorption and **(c)** CO_2 isotherms of LAG–HMI–20, LAG–4HICA–20, and LAG–4MICA–20 samples with CO_2 isotherms of HICA–20C and HICA–10A for comparison.

Table 4
^{1}H NMR determined linker exchange and sorption results for LAG-20 samples with other linkers.

Sample	Linker exchange (%)	S_{BET} (m^2/g)	V_{micro} (mL/g)	V_{total} (mL/g)	CO_2 uptake (mmol/g)
LAG – 4HICA – 20	45	402	0.15	0.43	0.75
LAG – 4MICA – 20	41	591	0.22	0.26	1.08
LAG – HMI – 20	20	961	0.36	0.68	0.62

4. Conclusions

Herein, we report on a successful implementation of ball-milling MALE for the ZIF–8 system by introducing a HICA polar ligand. Various reaction conditions were explored, and comparable linker exchange was achieved within 15 min, matching the results of the previously reported manual MALE process for ZIF–8 with HICA that required 8 h. This represents a shortening of the reaction time by 320% compared to the previously reported procedure, thus significantly enhancing the practical applicability of the technique. As anticipated, a general trend was observedl; higher milling frequency led to higher linker exchange accompanied by increased loss of crystallinity. The optimal conditions (20 Hz, 15 min) were then tested for MALE with four additional imidazole linkers that either have difficulty forming SOD phases or do not have known SOD phases. Notable exchange was observed for three selected imidazoles, and in the case of DCl, almost complete recrystallization into the RHO phase was observed. Various milder conditions were also tested for the 4 linkers, where the liquid-assisted (LAG)-MALE approach allowed for higher retention of the SOD framework at the cost of a slightly lower linker exchange.

Testing all the MALE samples for CO_2 sorption revealed that HICA–30C (63% exchange) exhibited nearly 3 times the uptake of HICA–10A (6% exchange). Furthermore, the 4MICA and 4HICA MALE samples with polar functional groups at position 4 in the imidazolate ring demonstrated significantly higher CO_2 affinity at lower pressures with a change in isotherm shape from a linear to a Langmuir-type isotherm, as observed for the solvothermally prepared ZIF–8 analogue using 4MICA. The difference in CO_2 affinity between samples based on functional groups at position 2 (HICA) and samples based on functional groups at position 4 (4MICA, 4HICA) indicates that the terminal ring position functionalization is the key to the preparation of SOD ZIF sorbents with high affinity for CO_2.

This work demonstrates that the MALE post-synthetic procedure holds the potential for quick functionalization of parent stable and commercially available ZIFs, with the caveat that, similar to the SALE procedure, it requires optimization for each ZIF/exchange linker system, but its speed allows for the optimization to be carried out within a short time frame, unlike the day-long SALE.

CRediT authorship contribution statement

Aljaž Škrjanc: Formal analysis, Methodology, Conceptualization, Writing – original draft. **Nataša Zabukovec Logar:** Writing – review & editing, Funding acquisition.

Declaration of competing interest

Nataša Zabukovec Logar is an editorial board member for Green Carbon and was not involved in the editorial review or the decision to publish this article. The authors declare that they have no known competing financial interests or personal relationships that could have appeared to influence the work reported in this paper.

Acknowledgments

We would like to thank Mojca Opresnik for SEM measurements, Edi Kranjc for PXRD, Jan Dežan for selected samples' preparation, and the Slovenian NMR center for granting access to the NMR equipment. We would also like to thank the Laboratory for Applied and Sustainable Chemistry, of the Institute Ruđer Bošković, for their help with the LAG MALE. This study was supported by the Slovenian Research and Innovation Agency [Grant No. P1–0021].

Appendix A. Supporting information

Supplementary data associated with this article can be found in the online version at doi:10.1016/j.greenca.2025.06.002.

References

[1] A. Phan, C.J. Doonan, F.J. Uribe-Romo, C.B. Knobler, M. Okeeffe, O.M. Yaghi, Synthesis, structure, and carbon dioxide capture properties of zeolitic imidazolate frameworks, Acc. Chem. Res. 43 (2010) 58–67.
[2] O.M. Yaghi, M.J. Kalmutzki, C.S. Diercks, Zeolitic imidazolate frameworks, in: O.M. Yaghi, M.J. Kalmutzki, C.S. Diercks (Eds.), Introduction to Reticular Chemistry: Metal-Organic Frameworks and Covalent Organic Frameworks, Wiley-VCH, Weinheim, 2019, pp. 463–479.
[3] A. Škrjanc, C. Byrne, N. Zabukovec Logar, Green solvents as an alternative to DMF in ZIF-90 synthesis, Molecules 26 (2021) 1573.
[4] C. Byrne, A. Ristić, S. Mal, M. Opresnik, N.Z. Logar, Evaluation of ZIF-8 and ZIF-90 as heat storage materials by using water, methanol and ethanol as working fluids, Crystals 11 (2021) 1422.
[5] K.S. Park, Z. Ni, A.P. Côté, J.Y. Choi, R.D. Huang, F.J. Uribe-Romo, H.K. Chae, M. O'Keeffe, O.M. Yaghi, Exceptional chemical and thermal stability of zeolitic imidazolate frameworks, Proc. Natl. Acad. Sci. USA 103 (2006) 10186–10191.
[6] S. Tanaka, Y. Tanaka, A simple step toward enhancing hydrothermal stability of ZIF-8, ACS Omega 4 (2019) 19905–19912.
[7] K. Villegas Domínguez, B. Delgado, A. Wilkin, S. Brar, M. Heitz, A. Avalos Ramirez, Study of adsorption interactions between nitrous oxide and zeolitic imidazolate framework-8 (ZIF-8) by molecular modeling, Catal. Today 388-389 (2022) 141–146.
[8] K.Q. Zhang, R. Wang, A critical review on new and efficient adsorbents for CO_2 capture, Chem. Eng. J. 485 (2024) 149495.

[9] W. Morris, B. Leung, H. Furukawa, O.K. Yaghi, N. He, H. Hayashi, Y. Houndonougbo, M. Asta, B.B. Laird, O.M. Yaghi, A combined experimental – computational investigation of carbon dioxide capture in a series of isoreticular zeolitic imidazolate frameworks, J. Am. Chem. Soc. 132 (2010) 11006–11008.
[10] H. Amrouche, S. Aguado, J. Pérez-Pellitero, C. Chizallet, F. Siperstein, D. Farrusseng, N. Bats, C. Nieto-Draghi, Experimental and computational study of functionality impact on sodalite-zeolitic imidazolate frameworks for CO_2 separation, J. Phys. Chem. C. 115 (2011) 16425–16432.
[11] W. Morris, N. He, K.G. Ray, P. Klonowski, H. Furukawa, I.N. Daniels, Y.A. Houndonougbo, M. Asta, O.M. Yaghi, B.B. Laird, A combined experimental-computational study on the effect of topology on carbon dioxide adsorption in zeolitic imidazolate frameworks, J. Phys. Chem. C. 116 (2012) 24084–24090.
[12] Y.T. Liao, S. Dutta, C.H. Chien, C.C. Hu, F.K. Shieh, C.H. Lin, K.C.W. Wu, Synthesis of mixed-ligand zeolitic imidazolate framework (ZIF-8-90) for CO_2 adsorption, J. Inorg. Organomet. Polym. Mater. 25 (2015) 251–258.
[13] M. Åhlén, A. Jaworski, M. Strømme, O. Cheung, Selective adsorption of CO_2 and SF_6 on mixed-linker ZIF-7–8 s: the effect of linker substitution on uptake capacity and kinetics, Chem. Eng. J. 422 (2021) 130117.
[14] Q.Q. Hou, Y. Wu, S. Zhou, Y.Y. Wei, J. Caro, H.H. Wang, Ultra-tuning of the aperture size in stiffened ZIF-8_cm frameworks with mixed-linker strategy for enhanced CO_2/CH_4 separation, Angew. Chem. Int. Ed. 58 (2019) 327–331.
[15] F. Hillman, H.K. Jeong, Linker-doped zeolitic imidazolate frameworks (ZIFs) and their ultrathin membranes for tunable gas separations, ACS Appl. Mater. Interfaces 11 (2019) 18377–18385.
[16] C.W. Tsai, J.W. Niemantsverdriet, E.H.G. Langner, Enhanced CO_2 adsorption in nano-ZIF-8 modified by solvent assisted ligand exchange, Microporous Mesoporous Mater. 262 (2018) 98–105.
[17] Z.F. Jiang, W.J. Xue, H.L. Huang, H.J. Zhu, Y.X. Sun, C.L. Zhong, Mechanochemistry-assisted linker exchange of metal-organic framework for efficient kinetic separation of propene and propane, Chem. Eng. J. 454 (2023) 140093.
[18] Y.W. Abraha, C.W. Tsai, J.W.H. Niemantsverdriet, E.H.G. Langner, Optimized CO_2 capture of the zeolitic imidazolate framework ZIF-8 modified by solvent-assisted ligand exchange, ACS Omega 6 (2021) 21850–21860.
[19] O. Karagiaridi, W. Bury, A.A. Sarjeant, C.L. Stern, O.K. Farha, J.T. Hupp, Synthesis and characterization of isostructural cadmium zeolitic imidazolate frameworks via solvent-assisted linker exchange, Chem. Sci. 3 (2012) 3256–3260.
[20] K. Kenyotha, K.C. Chanapattharapol, S. McCloskey, P. Jantaharn, Water Based synthesis of ZIF-8 assisted by hydrogen bond acceptors and enhancement of CO_2 uptake by solvent assisted ligand exchange, Crystals 10 (2020) 599.
[21] O. Karagiaridi, M.B. Lalonde, W. Bury, A.A. Sarjeant, O.K. Farha, J.T. Hupp, Opening ZIF-8: a catalytically active zeolitic imidazolate framework of sodalite topology with unsubstituted linkers, J. Am. Chem. Soc. 134 (2012) 18790–18796.
[22] C.J. Jin, S.L. Shi, S. Liao, S.M. Liu, S.Y. Xia, Y.P. Luo, S.H. Wang, H.M. Wang, C. Chen, Post-synthetic ligand exchange by mechanochemistry: toward green, efficient, and large-scale preparation of functional metal–organic frameworks, Chem. Mater. 35 (2023) 4489–4497.
[23] A. Škrjanc, A. Golobič, M. Mazaj, M. Huš, B. Likozar, N.Z. Logar, Green synthesis of functionalized sodalite ZIFs through mechanochemistry and their performance in CO_2 capture, Microporous Mesoporous Mater. 384 (2025) 113453.
[24] J.J. Zhong, H. Wang, Y.P. Liu, L.X. Qian, L. Yao, X.Q. Xing, G. Mo, Z.J. Chen, Z.H. Wu, Moisture-assisted synthesis and carbon dioxide capture performance of ZIF-L in methanol solution, Cryst. Growth Des. 23 (2023) 2561–2567.
[25] Z.H. Huang, E.S. Grape, J. Li, A.K. Inge, X.D. Zou, 3D electron diffraction as an important technique for structure elucidation of metal-organic frameworks and covalent organic frameworks, Coord. Chem. Rev. 427 (2021) 213583.
[26] M. Švegovec, A. Škrjanc, A. Krajnc, N.Z. Logar, Green synthesis approaches toward preparation of ZIF-76 and its thermal behavior, Cryst. Growth Des. 23 (2023) 3754–3760.
[27] L.S. Lai, Y.F. Yeong, N.C. Ani, K.K. Lau, A.M. Shariff, Effect of synthesis parameters on the formation of zeolitic imidazolate framework 8 (ZIF-8) nanoparticles for CO_2 adsorption, Part. Sci. Technol. 32 (2014) 520–528.
[28] A. Škrjanc, M. Opresnik, M. Gabrijelčič, A. Šuligoj, G. Mali, N. Zabukovec Logar, Impact of dye encapsulation in ZIF-8 on CO_2, water, and wet CO_2 sorption, Molecules 28 (2023) 7056.
[29] T. Johnson, M.M. Łozińska, A.F. Orsi, P.A. Wright, S. Hindocha, S. Poulston, Improvements to the production of ZIF-94; a case study in MOF scale-up, Green Chem. 21 (2019) 5665–5670.